Acta Crystallographica Section D
Biological Crystallography
ISSN 0907-4449

High-resolution crystal structure of the isolated ribosomal L1 stalk

S. Tishchenko,[a] A. Gabdulkhakov,[a] N. Nevskaya,[a] A. Sarskikh,[a] O. Kostareva,[a] E. Nikonova,[a] A. Sycheva,[b] S. Moshkovskii,[b] M. Garber[a] and S. Nikonov[a]*

[a]Institute of Protein Research, Russian Academy of Sciences, 142290 Pushchino, Moscow Region, Russian Federation, and [b]Orekhovich Institute of Biomedical Chemistry, Russian Academy of Medical Sciences, Moscow, Russian Federation

Correspondence e-mail: nikonov@vega.protres.ru

Received 23 March 2012
Accepted 4 May 2012

PDB Reference: ribosomal L1 stalk, 3u4m.

The crystal structure of the isolated full-length ribosomal L1 stalk, consisting of *Thermus thermophilus* ribosomal protein L1 in complex with a specific 80-nucleotide fragment of 23S rRNA, has been solved for the first time at high resolution. The structure revealed details of protein–RNA interactions in the L1 stalk. Analysis of the crystal packing enabled the identification of sticky sites on the protein and the 23S rRNA which may be important for ribosome assembly and function. The structure was used to model different conformational states of the ribosome. This approach provides an insight into the roles of domain II of L1 and helix 78 of rRNA in ribosome function.

1. Introduction

The L1 stalk consisting of ribosomal protein L1 and helices 76, 77 and 78 of the 23S rRNA is a functionally important region of the ribosome. For a long time, the high mobility of this ribosomal domain prevented an accurate determination of its three-dimensional structure within the ribosomal particles. The binding of EF-G trapped in the post-translocational state by the antibiotic fusidic acid contributed to the stabilization of the mobile elements of the ribosome and allowed a more complete model of the *Thermus thermophilus* ribosome that included the entire L1 stalk to be built at 3.6 Å resolution (Gao *et al.*, 2009).

For detailed analysis of the L1–rRNA interactions, a higher resolution structure is required. We have previously succeeded in determining the crystal structure of a hybrid complex (Nikulin *et al.*, 2003) between L1 from the archaeon *Sulfolobus acidocaldarius* and a specific 55-nucleotide (55 nt) fragment (Drygin & Zimmermann, 2000) of 23S rRNA from *T. thermophilus* at 2.65 Å resolution. Crystals of TthL1 complexed with the same rRNA fragment diffracted to a lower resolution than crystals of the hybrid complex. To improve the quality of the crystals of the native *T. thermophilus* complex, we varied the length of the RNA fragment. The best crystals were obtained for the complex of TthL1 with an 80-nucleotide (80 nt) fragment containing the full-length helix 78 instead of the shorter part in the 55 nt fragment. The presence of the entire helix 78 provided additional intermolecular RNA–RNA and RNA–protein contacts which stabilized the crystal structure and allowed a higher resolution model of the isolated ribosomal domain to be obtained. Here, we present the structure of the full-length *T. thermophilus* ribosomal L1 stalk at 2.0 Å resolution and analyze the details of the RNA–

Table 1
Data-collection and refinement statistics for TthL1–80 nt RNA.

The data were collected at 110 K. Values in parentheses are for the highest resolution shell.

Data collection	
Wavelength (Å)	1.5418
Space group	$P2_12_12_1$
Unit-cell parameters (Å)	a = 62.55, b = 68.90, c = 117.56
Resolution (Å)	20.67–2.00 (2.10–2.00)
Measured reflections	133242 (16594)
Unique reflections	33346 (4415)
Completeness (%)	94.5 (89.7)
Averaged multiplicity	3.99 (3.75)
Average $I/\sigma(I)$	19.14 (6.68)
$R_{\rm merge}$ (%)	5.2 (20.4)
Mosaicity (°)	0.17
Refinement	
Resolution (Å)	19.70–2.00 (2.07–2.00)
No. of reflections	33346 (2922)
R factor (%)	17.9 (20.4)
Free R factor (%)	20.8 (24.9)
Overall B factor (Å^2)	21.3
R.m.s. deviations	
Bond lengths (Å)	0.007
Bond angles (°)	1.007
Ramachandran plot (%)	
Most favoured	95.2
Additionally allowed	4.8

protein interactions and intermolecular contacts in the crystal of the complex.

2. Materials and methods

2.1. Plasmid construction

A DNA construct containing sequences for the gene of the 80 nt *T. thermophilus* rRNA fragment (Tth rRNA), the T7 promotor, a *Hin*dIII site and an *Xma*I site was prepared by PCR using overlapping primers and was inserted into the corresponding sites of the vector pUC18. The sequence of the cloned PCR product was verified by sequencing. The plasmid construct for *T. thermophilus* L1 (TthL1) has been described previously (Nikonova *et al.*, 2007).

2.2. Protein and RNA preparation

TthL1 was overproduced in *Escherichia coli* BL21 (DE3) cells. The protein was purified as described previously (Nikonov *et al.*, 1996). The purified protein was dialyzed into 350 m*M* NaCl, 50 m*M* Tris–HCl (pH 7.5 at 298 K), 5 m*M* $MgCl_2$ and concentrated to 5–6 mg ml^{-1} using Vivaspin concentrators.

The 80 nt Tth rRNA fragment was obtained *in vitro* by transcription with T7 RNA polymerase from linearized plasmid DNA. RNA was purified on denaturing (6 *M* urea) 10%(*w*/*v*) acrylamide gels (19:1 acrylamide:bisacrylamide) using 90 m*M* Tris–acetate pH 7.8, 2 m*M* Na_2EDTA as the running buffer. The RNA was eluted with 50 m*M* Tris–HCl (pH 7.5 at 298 K), 2 m*M* Na_2EDTA, purified by anion-exchange (DEAE Sepharose) chromatography, precipitated using ethanol and dissolved in water to a concentration of 4–5 mg ml^{-1}.

2.3. Crystallization of the L1–rRNA complex

The RNA fragment was heated to 333 K for 10 min and incubated at 277 K for 10 min. To form the TthL1–RNA complex, preparations of the RNA fragment and the protein were mixed in equimolar amounts and incubated for 30 min at room temperature.

Crystallization experiments were performed at room temperature using the hanging-drop vapour-diffusion method on siliconized glass cover slides in Linbro plates. Drops were made by mixing 2 µl of the complex solution with 0.5 µl 1.4% polyacrylic acid 5100 sodium salt and 2 µl 2.5 *M* ammonium sulfate, 0.01 *M* magnesium acetate, 0.05 *M* MES pH 5.6 (condition No. 2 of Natrix from Hampton Research). The well solution consisted of 2.2 *M* ammonium sulfate, 0.05 *M* MES pH 5.6. Crystals appeared after 3–4 d and grew to maximum dimensions of 0.1 × 0.2 × 0.6 mm within 1–2 weeks. Prior to freezing in liquid nitrogen, the crystals were transferred into 2.4 *M* sodium malonate pH 6.0.

2.4. Data collection and structure determination

Diffraction data for the TthL1–rRNA complex were collected from a single crystal using an in-house Proteum X8 generator (Bruker) equipped with a MAR345 image-plate detector (MAR Research, Germany). Data were processed and merged with the *XDS* package (Kabsch, 2010). The crystals belonged to space group $P2_12_12_1$, with unit-cell parameters a = 62.6, b = 68.9, c = 117.6 Å and one molecule in the asymmetric unit.

The structure was solved by molecular replacement with *Phaser* (McCoy *et al.*, 2005) using Ser179Cys TthL1 (PDB entry 1ad2; Unge *et al.*, 1997) and the 55 nt fragment of 23S rRNA (PDB entry 1mzp; Nikulin *et al.*, 2003) as separate domains as search models. The initial model was subjected to crystallographic refinement, initially with *REFMAC*5 (Murshudov *et al.*, 2011) and subsequently with *PHENIX* (Adams *et al.*, 2002). Manual rebuilding of the model was carried out in *Coot* (Emsley & Cowtan, 2004). The final model of the complex, which was refined to an R factor of 17.9% and an $R_{\rm free}$ of 20.8% at 2.0 Å resolution, includes 228 amino acids, 80 nucleotides, 203 water molecules, five magnesium ions, two chloride ions, five sodium ions, two sulfate ions and seven malonate ions. The quality of the model was checked using *PROCHECK* (Laskowski *et al.*, 1993) and *WHAT_CHECK* (Hooft *et al.*, 1996) and showed that 95.2% of the residues have the most favoured conformations, while the remainder are in the additionally allowed region. Data-collection and refinement statistics are summarized in Table 1. The coordinates and structure factors have been deposited in the Protein Data Bank (PDB entry 3u4m). Figures were prepared using *PyMOL* (http://www.pymol.org).

2.5. SPR experiments

Real-time monitoring of the interactions between TthL1 and fragments of 23S rRNA and mRNA containing the specific L1-binding sites was performed by SPR experiments (Katsamba *et al.*, 2002) using the ProteOn XPR36 interaction

array system (Bio-Rad, USA). Binding experiments were performed as reported previously (Kostareva *et al.*, 2011) with a minor modification (the running buffer contained 430 m*M* instead of 350 m*M* NaCl). Kinetic analysis was performed by globally fitting curves describing a simple 1:1 bimolecular model to the set of five sensorgrams.

3. Results

3.1. Overall description of the TthL1–80 nt rRNA structure

The components and the overall structure of the TthL1–RNA complex are shown in Fig. 1. The structure contains the entire L1 protein (Fig. 1*a*) and 80 nt fragment of 23S rRNA (Fig. 1*d*). The structure of the complex has the shape of a trigonal prism with a base of 50 × 65 × 75 Å and a height of approximately 40 Å. Domain I, domain II and helix 78 (H78) form the lateral edges of the prism. The axis of helix 76 is approximately perpendicular to the base of the prism and passes through its centre.

3.2. Structure of the L1 protein

Ribosomal protein L1 (Fig. 1*b*) consists of two domains connected by a hinge region, with the N- and C-termini close to each other in domain I. Domain I contains a four-stranded antiparallel β-sheet that is flanked by two α-helices on one side and is exposed on the other side. Domain II has an overall

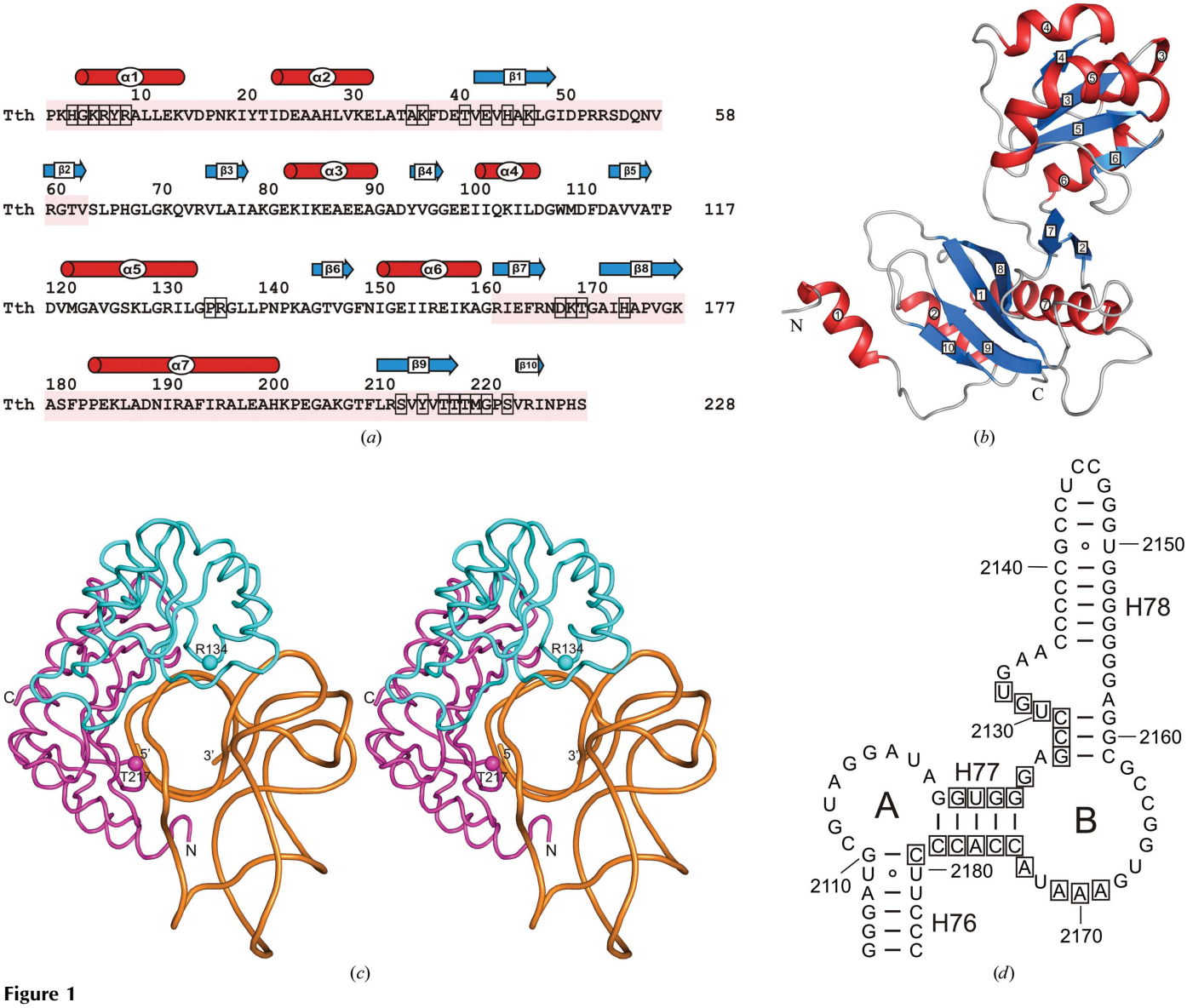

Figure 1
Components of the TthL1–rRNA complex. (*a*) Sequence of the *T. thermophilus* L1 protein. Residues of domain I are shown with a pink background. Residues interacting with RNA are boxed. α-Helices are shown as red cylinders and β-strands as blue arrows. (*b*) Ribbon diagram of TthL1. α-Helices (red) and β-strands (blue) are numbered. (*c*) Stereoview of the TthL1–RNA complex. The protein is shown in magenta (domain I) and cyan (domain II) and the RNA phosphate trace is shown in gold. The central residues of the RNA-contacting sites in both domains are shown as balls. (*d*) Secondary structure of the 80 nt 23S rRNA fragment from *T. thermophilus*. Sequence positions and helices are numbered according to *E. coli* 23S rRNA. Nucleotides interacting with the protein are boxed.

Rossmann-fold topology and contains two helices on each side of a four-stranded parallel β-sheet. The link between the two domains consists of two oppositely directed polypeptide chains and serves as a hinge for domain movements. The structure of each domain is essentially preserved between the current structure of TthL1–rRNA and the previously determined structure of TthL1–mRNA (Tishchenko *et al.*, 2006). The mean r.m.s. deviations are 0.346 and 0.833 Å for all C^{α} atoms of domain I (residues 1–65 and 160–228) and of domain II (residues 71–158), respectively. The lower conformational stability of domain II results from the mobility of helix α4. Similarly to L1 in other TthL1–RNA complexes (Nevskaya *et al.*, 2006; Tishchenko *et al.*, 2006), the two domains of this protein are separated from each other and demonstrate an 'open' conformation. In this conformation, the relative arrangement of the domains can vary by a rotation of up to about 10° in different complexes.

3.3. Structure of the 23S rRNA fragment

The fragment of 23S rRNA used contains 80 nucleotides and includes the entire helices 77 and 78, a shortened version of helix 76 and interconnecting loops A and B (Fig. 1*d*). Helices 76 and 77 of 23S rRNA are joined in one helical structure with the noncanonical base pair G2125·A2173 at its end and the bulged loop A (C2111–A2119) at the centre (Fig. 2). Loop B (A2126, G2162–U2172) interconnects helices 77 and 78. The bases of G2127 and U2172 are pulled out of the stacking lines of helix 77 to stack on bases in helix 78 and loop B and to form canonical base pairs with C2161 and A2117, respectively. The ribose moieties of A2126 and G2127 are approximately perpendicular to each other. As a result, the RNA backbone bends sharply at the phosphate group of G2127. This turn is stabilized by a network of hydrogen bonds, including those to the base moiety of the highly conserved A2173.

Helix 78 consists of two approximately perpendicular parts owing to a sharp bend at the phosphate group of U2132, the base of which is largely exposed. Stacking interactions and a network of hydrogen bonds stabilize this bend. The short part of H78 contains three canonical base pairs (G2127–C2161, C2128–G2160 and C2129–G2159) capped by U2130. The long part of helix 78 starts with three noncanonical base pairs in which the bases of G2133 and A2158 are interchanged in the stacking lines of the helix (Fig. 2*b*).

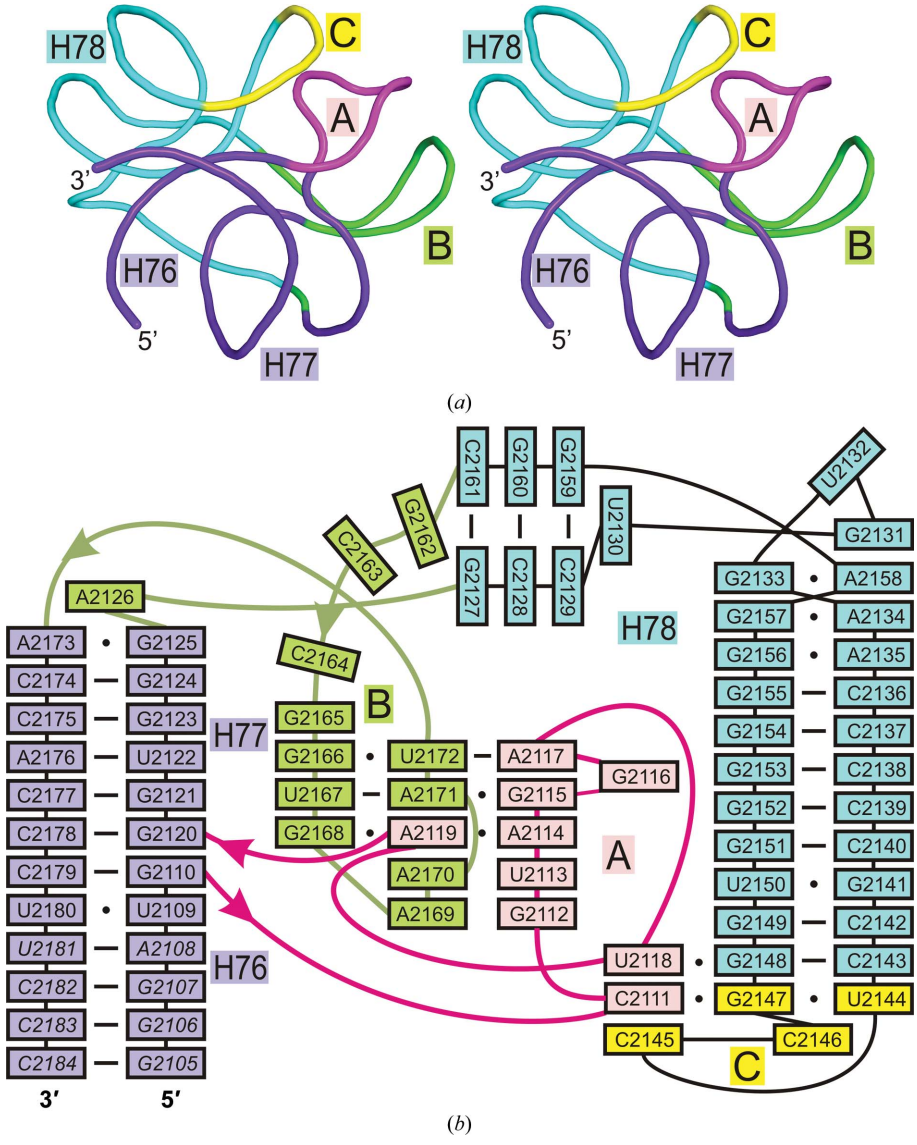

Figure 2
Structure of the RNA fragment. RNA is coloured according to secondary structure. (*a*) Stereoview of the RNA fragment. (*b*) Diagram of stacking interactions within the RNA fragment.

The mutual arrangement of the interconnecting loops A and B and the closing loop C of helix 78 is strongly stabilized by a large number of contacts (Fig. 2). The closing loop C and the interconnecting loop A are linked by two triples (U2144·G2147·C2111 and C2143–G2148·U2118), a network of hydrogen bonds and stacking interactions of the bases of C2111, U2118 and C2145. Loops A and B are linked by three base triples (A2114·A2119·G2168, G2115·A2171–U2167, A2117–U2172·G2166), which interact *via* an extensive network of hydrogen bonds. The bases of the interacting loops A and B form three stacking lines, (i) G2112, U2113, A2114, G2115 and A2117; (ii) A2169, A2170, A2119, A2171 and U2172; and (iii) G2168, U2167, G2166, G2165, C2164, C2163 and G2162, the last of which is bifurcated into lines G2127, C2128, C2129 and C2161, G2160, G2159.

Table 2
Lengths of the conserved L1–RNA hydrogen bonds.

L1–RNA hydrogen bond	Bond length (Å)
Glu42 OE1···N2 G2123	3.09
Glu42 OE2···O2′ G2124	2.68
Asp166 OD2···N2 G2121	2.92
Thr217 OG1···O2′ G2124	2.77
Thr217 O···N2 G2124	3.13
Thr217 O···O2′ C2175	3.28
Met218 SD···O2′ C2174	3.21
Gly219 O···O2′ C2175	2.64

The closing loop of helix 78 is in the close vicinity of the middle part of helices 76–77. The phosphate groups of U2109 and G2110 intrude into the shallow grove of H78 and form direct and water-mediated hydrogen bonds with its bases and riboses. In general, this 23S rRNA fragment represents a very compact structure with an approximately spherical shape.

Superposition of the present structure onto that of the L1 stalk of the 70S ribosome at 3.6 Å resolution (Gao *et al.*, 2009) yielded r.m.s. deviations of 1.02 Å for all P atoms of RNA and 0.92 Å for all C^{α} atoms of the protein. It follows that the structure of TthL1 in complex with the 23S rRNA fragment solved at high resolution can be used for detailed analysis of the protein–RNA interactions in the ribosomal L1 stalk.

3.4. Protein–RNA interactions

Upon complex formation, 1450 $Å^2$ of the protein surface and 1483 $Å^2$ of the RNA surface are buried. There are two sites of protein–RNA interaction between TthL1 and the 23S rRNA. One of the sites is extensive (about 90% of the contact area) and involves residues of domain I of L1 and nucleotides of H77 and the short part of H78. Domain I contacts RNA *via* the N-terminal helix (α1) and the slightly concave surface formed by the inner face of the β-sheet consisting of strands β1, β8, β9 and β10 and loops α2–β1, β7–β8 and β9–β10 (Fig. 1*a*). The residues of helix α1 interact with one strand of H77 and one strand of H78 through the ribose-phosphate moiety, with the exception of U2132 (Fig. 1*d*). The base of this nucleotide is rotated out of the stacking lines of H78 to interact with the side chain of Arg8. The concave region of domain I mimicks the turn of H77 and interacts with its nucleotides (Fig. 1*c*). Helix 77 contacts TthL1 primarily *via* the ribose-phosphate backbone. The structure of the contact region formed by domain I and helices 77 and 78 is stabilized by 23 hydrogen bonds, eight of which are inaccessible to the solvent (Table 2). Three of these inaccessible hydrogen bonds are base-specific.

A positively charged sodium ion found in the RNA–protein interface is of profound interest (Fig. 3). This ion is inaccessible to the solvent and is coordinated by RNA and protein groups, with seven ligands in the first coordination sphere. The ligands are the O atoms of three amino-acid residues (Glu42, Thr216 and Thr217) of the conserved amino-acid cluster of the protein as well as those of two nucleotides (C2175 and A2176) of the RNA fragment. The position of this ion coincides with the position of a potassium ion found previously in the TthL1–mRNA interface (Nevskaya *et al.*, 2006). This positively charged ion obviously plays an important role in the stabilization of L1–RNA complexes.

The second site of RNA–protein interaction is restricted and involves residues of domain II and nucleotides of loop B. The contact surface of domain II is approximately perpendicular to the contact surface of domain I and involves two highly conserved residues (Pro133 and Arg134). Three solvent-accessible L1–RNA hydrogen bonds formed by Arg134 to the phosphate groups of A2170 and A2171 and several van der Waals contacts stabilize this site.

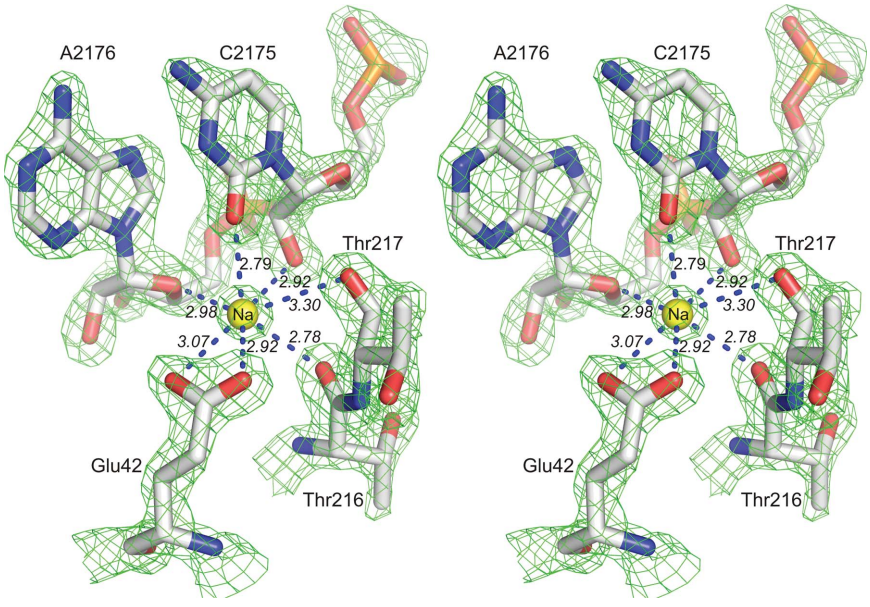

Figure 3
A stereoview showing the $2F_o - F_c$ map at 2.0 Å resolution contoured at 2.5σ in the region of a positively charged sodium ion in the RNA–protein interface.

The RNA-binding surface of the protein appears as a hollow (Fig. 1*c*) parallel to the axis of helices 76–77. The bottom of the hollow is uncharged and contains the triad Thr217-Met218-Gly219. This triad forms a tight contact with a flat region of the RNA, whereas the sides of the hollow contain positively charged residues which presumably interact with the phosphate groups of the ribose-phosphate backbone. Depending on their localization on the sides of the hollow, the positively charged residues can be grouped into two clusters. One cluster includes His44, Lys46, Arg52, Arg164, Lys167, His172 and Arg210. All of these residues are essentially located on the β-sheet surface. Residues Arg129 and Arg134 of domain II can also be assigned to this cluster. The other cluster is formed by residues Lys2, His3, Lys5, Arg6, Lys36, Lys70 and Lys177. Most of these residues belong to helix α1. Practically all of the interactions formed by positively charged

Table 3
Apparent kinetic constants and contact areas for the interaction of TthL1 with rRNA and mRNA.

RNA	k_{ass} (M^{-1} s^{-1})	k_{diss} (s^{-1})	K_d (M)	$S_{contact\ area}$ (Å^2)
80 nt 23S rRNA	5.64×10^5	1.21×10^{-6}	2.14×10^{-12}	1466
55 nt 23S rRNA	2.03×10^5	1.84×10^{-5}	9.06×10^{-11}	1405
mRNA	6.06×10^3	5.19×10^{-4}	8.58×10^{-8}	1256

amino-acid residues of the protein and phosphate groups of the rRNA fragment are accessible to the solvent and can exchange hydrogen bonds with water molecules, while the thickness of the hydrogen shell at the bottom of the hollow is minimal. Such a distribution of neutral and positively charged residues favours protein–RNA recognition and binding. It is possible that electrostatic interactions between the positively charged edges of the hollow and the negatively charged phosphate groups of rRNA play a key role in the mutual orientation of the partners, whereas the hydrogen bonds formed by polar atoms located at the bottom of the hollow with RNA bases and riboses provide stability to the complex.

3.5. Crystal packing

Depending on the shapes of the protein and RNA molecules, three types of contacts are possible between adjacent protein–RNA complexes in a crystal: RNA–RNA, protein–protein and RNA–protein contacts.

All three types of contact are realised in the crystals of TthL1–80 nt rRNA (Fig. 4). Owing to RNA–RNA interactions, the RNA molecules form rows parallel to the *a* axis of the crystal unit cell. The end view of these rows has the appearance of symmetric dumbbells perpendicular to each other. Contacts between RNA molecules in the row are realised through the shallow groove of helix 78 and a short part of H78. There are no RNA–RNA contacts between neighbouring rows; the protein is needed to fill the gaps between them. The protein molecule connects two RNA rows (Fig. 4). One RNA–protein contact is formed by the N-termini of helices $\alpha3$, $\alpha5$ and $\alpha6$ of domain II and the nucleotides of helix 78. Contacts between the protein and another row are formed by the $\alpha1$–$\alpha2$ loop and helix $\alpha2$ of domain I and the shallow groove of helix 76 of the RNA. Two neighbouring protein molecules also form a tight contact. This protein–protein contact is realised through two loops of domain I ($\alpha2$–$\beta1$ and $\beta8$–$\alpha7$) and strand $\beta4$ and helix $\alpha4$ of domain II. All of the contacts are mainly flat and are stabilized by direct and water-mediated hydrogen bonds.

Thus, analysis of crystal packing makes it possible to identify several sticky sites on the RNA (the long part of helix 78) and protein (domain II) surfaces which could be involved in ribosome function. These sites do not participate in protein–RNA interactions within the complex.

4. Discussion

4.1. Influence of nonconserved interactions on L1–RNA affinity

We have previously shown that ribosomal protein L1 recognizes the same structural motif in the specific fragments of 23S rRNA (55 nt) and its mRNA (49 nt) (Nevskaya *et al.*, 2005). Analysis of the structures of L1 in complex with the 36 nt fragment of mRNA (Tishchenko *et al.*, 2006) and with the 80 nt fragment of 23S rRNA (this work) confirms this conclusion. Nevertheless, kinetic data on L1–RNA interactions obtained by surface plasmon resonance experiments show that L1 has different affinities for all of these RNAs (Table 3).

The 55 nt fragment of rRNA contains helix 77, interconnecting loops A and B and shortened versions of helices 76 and 78, while the 80 nt fragment includes the entire helix 78. The lack of a large part of H78 slightly reduces the surface of the 55 nt fragment which interacts with helix $\alpha1$ of the protein. This decreases the protein–RNA affinity by about 50-fold, although most of the contacts are still preserved in the RNA–protein interface and the protein interacts specifically with the RNA fragment.

In mRNA fragments which specifically bind L1 there are no structural elements that correspond to H78 and loop B of rRNA. The lack of helix 78 and the smaller contact area formed by domain I compared with the 80 nt rRNA fragment decrease the apparent association rate constant in the case of the 55 nt rRNA fragment to only a small extent. On the other hand, the additional lack of loop B in the mRNA fragment and the absence of a contact with domain II of L1 impair protein–RNA recognition dramatically (Table 3). As a general rule, the energy of intermolecular interactions is proportional to the surface area that they bury (Chothia & Janin, 1975). Nevertheless, the changes in the areas of the contact surfaces in L1–RNA complexes are not

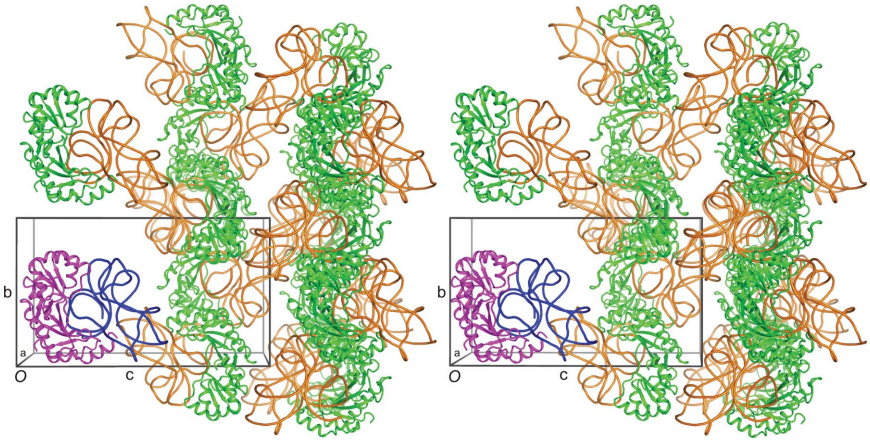

Figure 4
Packing of complexes in the TthL1–80 nt rRNA crystal. The complex in the asymmetric unit of the crystal is shown in magenta (TthL1) and blue (rRNA).

sufficient for the observed decrease of L1–RNA affinity in regulatory complexes. The same result has been obtained previously from an examination of the complexes formed by ribosomal protein S8 with specific 16S rRNA and mRNA fragments (Merianos *et al.*, 2004). It is worth noting that loop B of rRNA interacts with domain II of L1 and forms the second contact site, which is separated and remote from the main site of interaction. It may be suggested that the presence of such a site is needed for the mutual orientation of the partners and is more important for protein–RNA recognition and affinity than a small decrease in contact area.

4.2. Possible roles of helix 78 of 23S rRNA and domain II of L1 in ribosome function

Cryo-EM (Valle *et al.*, 2003; Agirrezabala *et al.*, 2008), X-ray (Schuwirth *et al.*, 2005; Selmer *et al.*, 2006; Jin *et al.*, 2011) and single-molecule FRET (Cornish *et al.*, 2009) studies show at least three different orientations of the L1 stalk relative to the body of the 50S subunit: fully closed, half-closed and open. In the fully closed and half-closed conformations the L1 stalk contacts the elbow of tRNA. Superposition of the structures of the L1–rRNA complex (this work) and the L1 stalk of the ribosome in the closed state (Jin *et al.*, 2011) shows that the tRNA elbow penetrates into the interdomain cavity of the L1 protein and interacts with loop $\alpha5$–$\beta6$ of domain II and helix 76 of rRNA. These contacts were also found for the half-closed conformation of the L1 stalk. Hence, domain II of L1 is probably essential for the escape of tRNA from the ribosome. Modelling the open conformation of the L1 stalk using the structures of vacant ribosomes (Schuwirth *et al.*, 2005), the present L1–rRNA complex and protein L9 (Hoffman *et al.*, 1994) shows that the shallow groove of helix 78 is located close to the C-terminal domain of L9 and could interact with it. It is possible that interactions between helix 78 and protein L9 promote the removal of tRNA from the ribosome.

This work was supported by the Russian Academy of Sciences (RAS), the Russian Foundation for Basic Research and the Program of RAS on Molecular and Cellular Biology. SPR experiments were performed at the Human Proteome Shared Facility Center of the Institute of Biomedical Chemistry, Moscow, Russia.

References

Adams, P. D., Grosse-Kunstleve, R. W., Hung, L.-W., Ioerger, T. R., McCoy, A. J., Moriarty, N. W., Read, R. J., Sacchettini, J. C., Sauter, N. K. & Terwilliger, T. C. (2002). *Acta Cryst.* D**58**, 1948–1954.
Agirrezabala, X., Lei, J., Brunelle, J. L., Ortiz-Meoz, R. F., Green, R. & Frank, J. (2008). *Mol. Cell*, **32**, 190–197.
Chothia, C. & Janin, J. (1975). *Nature (London)*, **256**, 705–708.
Cornish, P. V., Ermolenko, D. N., Staple, D. W., Hoang, L., Hickerson, R. P., Noller, H. F. & Ha, T. (2009). *Proc. Natl Acad. Sci. USA*, **106**, 2571–2576.
Drygin, D. & Zimmermann, R. A. (2000). *RNA*, **6**, 1714–1726.
Emsley, P. & Cowtan, K. (2004). *Acta Cryst.* D**60**, 2126–2132.
Gao, Y.-G., Selmer, M., Dunham, C. M., Weixlbaumer, A., Kelley, A. C. & Ramakrishnan, V. (2009). *Science*, **326**, 694–699.
Hoffman, D. W., Davies, C., Gerchman, S. E., Kycia, J. H., Porter, S. J., White, S. W. & Ramakrishnan, V. (1994). *EMBO J.* **13**, 205–212.
Hooft, R. W. W., Vriend, G., Sander, C. & Abola, E. E. (1996). *Nature (London)*, **381**, 272.
Jin, H., Kelley, A. C. & Ramakrishnan, V. (2011). *Proc. Natl Acad. Sci. USA*, **108**, 15798–15803.
Kabsch, W. (2010). *Acta Cryst.* D**66**, 125–132.
Katsamba, P. S., Park, S. & Laird-Offringa, I. A. (2002). *Methods*, **26**, 95–104.
Kostareva, O., Tishchenko, S., Nikonova, E., Kljashtorny, V., Nevskaya, N., Nikulin, A., Sycheva, A., Moshkovskii, S., Piendl, W., Garber, M. & Nikonov, S. (2011). *J. Mol. Recognit.* **24**, 524–532.
Laskowski, R. A., MacArthur, M. W., Moss, D. S. & Thornton, J. M. (1993). *J. Appl. Cryst.* **26**, 283–291.
McCoy, A. J., Grosse-Kunstleve, R. W., Storoni, L. C. & Read, R. J. (2005). *Acta Cryst.* D**61**, 458–464.
Merianos, H. J., Wang, J. & Moore, P. B. (2004). *RNA*, **10**, 954–964.
Murshudov, G. N., Skubák, P., Lebedev, A. A., Pannu, N. S., Steiner, R. A., Nicholls, R. A., Winn, M. D., Long, F. & Vagin, A. A. (2011). *Acta Cryst.* D**67**, 355–367.
Nevskaya, N., Tishchenko, S., Gabdoulkhakov, A., Nikonova, E., Nikonov, O., Nikulin, A., Platonova, O., Garber, M., Nikonov, S. & Piendl, W. (2005). *Nucleic Acids Res.* **33**, 478–485.
Nevskaya, N., Tishchenko, S., Volchkov, S., Kljashtorny, V., Nikonova, E., Nikonov, O., Nikulin, A., Köhrer, C., Piendl, W., Zimmermann, R., Stockley, P., Garber, M. & Nikonov, S. (2006). *J. Mol. Biol.* **355**, 747–759.
Nikonova, E. Y., Volchkov, S. A., Kljashtorny, V. G., Tishchenko, S. V., Kostareva, O. S., Nevskaya, N. A., Nikonov, O. S., Gabdoulkhakov, A. G., Nikulin, A. D., Davydova, N. L., Streltsov, V. A., Garber, M. B. & Nikonov, S. V. (2007). *Mol. Biol. (Mosk.)*, **41**, 688–696.
Nikonov, S., Nevskaya, N., Eliseikina, I., Fomenkova, N., Nikulin, A., Ossina, N., Garber, M., Jonsson, B. H., Briand, C., Al-Karadaghi, S., Svensson, A., Aevarsson, A. & Liljas, A. (1996). *EMBO J.* **15**, 1350–1359.
Nikulin, A., Eliseikina, I., Tishchenko, S., Nevskaya, N., Davydova, N., Platonova, O., Piendl, W., Selmer, M., Liljas, A., Drygin, D., Zimmermann, R., Garber, M. & Nikonov, S. (2003). *Nature Struct. Biol.* **10**, 104–108.
Schuwirth, B. S., Borovinskaya, M. A., Hau, C. W., Zhang, W., Vila-Sanjurjo, A., Holton, J. M. & Cate, J. H. D. (2005). *Science*, **310**, 827–834.
Selmer, M., Dunham, C. M., Murphy, F. V. IV, Weixlbaumer, A., Petry, S., Kelley, A. C., Weir, J. R. & Ramakrishnan, V. (2006). *Science*, **313**, 1935–1942.
Tishchenko, S., Nikonova, E., Nikulin, A., Nevskaya, N., Volchkov, S., Piendl, W., Garber, M. & Nikonov, S. (2006). *Acta Cryst.* D**62**, 1545–1554.
Unge, J., Al-Karadaghi, S., Liljas, A., Jonsson, B. H., Eliseikina, I., Ossina, N., Nevskaya, N., Fomenkova, N., Garber, M. & Nikonov, S. (1997). *FEBS Lett.* **411**, 53–59.
Valle, M., Zavialov, A., Sengupta, J., Rawat, U., Ehrenberg, M. & Frank, J. (2003). *Cell*, **114**, 123–134.